Mon. Not. R. Astron. Soc. **386,** 1380–1397 (2008) doi:10.1111/j.1365-2966.2008.12926.x

CCD photometric and mass function study of nine young Large Magellanic Cloud star clusters

B. Kumar,[1,2⋆] R. Sagar[2⋆] and J. Melnick[3⋆]

[1]*Departamento de Física, Universidad de Concepción, Casilla 160-C, Concepción, Chile*
[2]*Aryabhatta Research Institute of Observational Sciences, Manora Peak, Nainital 263 129, India*
[3]*European Southern Observatory, Alonso de Córdova 3107, Casilla 19001, Vitacura, Santiago, Chile*

Accepted 2008 January 7. Received 2007 December 19; in original form 2007 November 28

ABSTRACT

We present a CCD photometric and mass function study of nine young Large Magellanic Cloud star clusters, namely NGC 1767, 1994, 2002, 2003, 2006, SL 538, NGC 2011, 2098 and 2136. *BV RI* data, reaching down to $V \sim 21$ mag, were collected from the 3.5-m NTT/EFOSC2 in subarcsec seeing conditions. For NGC 1767, 1994, 2002, 2003, 2011 and 2136, broad-band photometric CCD data are presented for the first time. Seven of the nine clusters have ages between 16 and 25 Myr, and the other two have ages of 32 ± 4 Myr (NGC 2098) and 90 ± 10 Myr (NGC 2136). For the seven youngest clusters, the age estimates based on a recent model and the integrated spectra are found to be systematically lower ($\sim$10 Myr) than the present estimates. In the mass range $\sim$2–12 $M_{\odot}$, the mass function slopes for eight out of nine clusters were found to be similar, with the value of γ ranging from -1.90 ± 0.16 to -2.28 ± 0.21. For NGC 1767 the slope is flatter, with $\gamma = -1.23 \pm 0.27$. Mass segregation effects are observed for NGC 2002, 2006, 2136 and 2098. This is consistent with the findings of Kontizas and colleagues for NGC 2098. The presence of mass segregation in these clusters could be an imprint of the star formation process, as their ages are significantly smaller than their dynamical evolution time. The mean mass function slope of $\gamma = -2.22 \pm 0.16$ derived for a sample of 25 young ($\leqslant$100 Myr) dynamically unevolved Large Magellanic Cloud stellar systems provides support for the universality of the initial mass function in the intermediate-mass range $\sim$2–12 $M_{\odot}$.

Key words: galaxies: clusters: general – Magellanic Clouds.

1 INTRODUCTION

The distribution of stellar masses that forms in one star formation event in a given volume of space is called the initial mass function (IMF). Some theoretical studies predict that the IMF should vary with the pressure and temperature of the star-forming cloud in such a way that higher-temperature regions ought to produce higher average stellar masses, whereas other studies reach exactly the opposite conclusion (see Larson 1998; Elmegreen 2000, and references therein). It is therefore of upmost importance to have a detailed knowledge of the IMF shape in different star-forming environments, and to determine whether or not the IMF is universal in time and space. In order to ascertain this, within a galaxy the young (age $\leqslant$100 Myr) star clusters of different ages, abundances etc. need to be observed, as they contain dynamically unevolved, (almost) coeval sets of stars at the same distance with the same metallicity. For a number of reasons, the populous young star clusters of the Large Magellanic Clouds (LMC) are the most suitable objects for investigating the IMF. They contain physical conditions, for example stellar richness, metallicity and mass ranges, not present in our Galaxy (see Sagar 1993, 1995, and references therein). Unlike the Galactic counterparts, where corrections for interstellar absorption are not always trivial, as the absorption can be large as well as variable (Sagar 1987; Yadav & Sagar 2001; Kumar et al. 2004), for LMC star clusters the absorption is relatively small and its treatment is therefore not a problem. Furthermore, choosing young (age $\leqslant$ 100 Myr) clusters reduces the effects of dynamical evolution on their mass function (MF). The present-day MF of these stellar systems can therefore be considered as the IMF. The study of young LMC star clusters is thus important for providing the answer to the question of the universality of the IMF. Both ground and *Hubble Space Telescope* (*HST*) observations have therefore been obtained (see Sagar & Richtler 1991; Brocato, Di Carlo & Menna 2001; Matteucci et al. 2002, and references therein) for a few of the large number of young LMC star clusters (Bica et al. 1999). The potential offered by these observations has not been fully utilized as a large fraction of the clusters is still unobserved.

⋆E-mail: bkumar@astro-udec.cl (BK); sagar@aries.ernet.in (RS); jmelnick@eso.org (JM)

Table 1. Preliminary information about the clusters under study. Cluster identifications are from Sulentic et al. (1973) (with acronym NGC) and Shapley & Lindsay (1963) (with acronym SL). The coordinates, major and minor diameters and position angle (P.A.) are taken from Bica et al. (1999), and the age and membership of a pair (mP) or multiple (mM) system, along with group number given in brackets in the last column, are taken from Dieball et al. (2002). All the clusters are of type C, indicating higher stellar density (Bica & Schmitt 1995).

Clusters	α_{J2000} (h m s)	δ_{J2000} (° ′ ″)	D_{maj} (arcmin)	D_{min} (arcmin)	P.A. (°)	Age (Myr)	Remarks
NGC 1767	4 56 27	−69 24 12	1.30	1.20	30	0–30	mM(39)
NGC 1994	5 28 21	−69 08 30	1.60	1.50	170	10–30	mM(275)
NGC 2002	5 30 21	−66 53 02	1.90	1.70	20	10–30	
NGC 2003	5 30 54	−66 27 59	1.70	1.40	70	10–30	mP(297)
SL538	5 31 18	−66 57 28	1.40	1.40		18±2	mP(303)
NGC 2006	5 31 19	−66 58 22	1.60	1.40	140	22.5±2.5	mP(303)
NGC 2011	5 32 19	−67 31 16	1.00	1.00		10–30	mP(320)
NGC 2098	5 42 30	−68 16 29	2.20	2.00	140	10–30	
NGC 2136	5 52 59	−69 29 33	2.80	2.50	140	70–200	mP(456)

In this paper we derive MF slopes using new broad-band *BVRI* CCD photometric observations of the stars in nine young LMC star clusters, namely NGC 1767, 1994, 2002, 2003, 2006, SL 538, NGC 2011, 2098 and 2136. Their integrated photometric colours indicate that all of them belong to SWB (Searle, Wilkinson & Bagnuolo 1980) class 0 or I, and hence are very young, with ages $\leqslant$30 Myr (Elson & Fall 1985; Bica et al. 1996), except for NGC 2136, which belongs to SWB class III, indicating an age between 70 and 200 Myr. Table 1 lists the relevant information available prior to this study. All of the clusters are rich, indicating a high stellar density (Bica & Schmitt 1995), and are thus highly suitable for MF study. With the exception of NGC 2011, all are elliptical in size, with major axis diameters ranging from 1.3 to 2.8 arcmin. Except for NGC 2002 and 2098, all the clusters are candidate members of either a pair or a multiple system (see Dieball, Mueller & Grebel 2002). The locations of the target clusters are shown in Fig. 1. Most of them lie towards the northeast side of the LMC bar, which harbours young star-forming regions in contrast to the intermediate-age (1–3 Gyr) cluster field of the bar. NGC 1767 lies southwest of the LMC bar. Being spread over a wide region ($\sim 5^\circ \times 10^\circ$), the sample may reflect different star-forming environments. It is therefore suitable for testing the universality of the IMF. When CCD observations were carried out in 1990, no detailed photometric observations or MF studies had been published. However, since then some CCD photometric observations have been published for a few of the clusters under study. A brief description of the previous work on the clusters under study is given below.

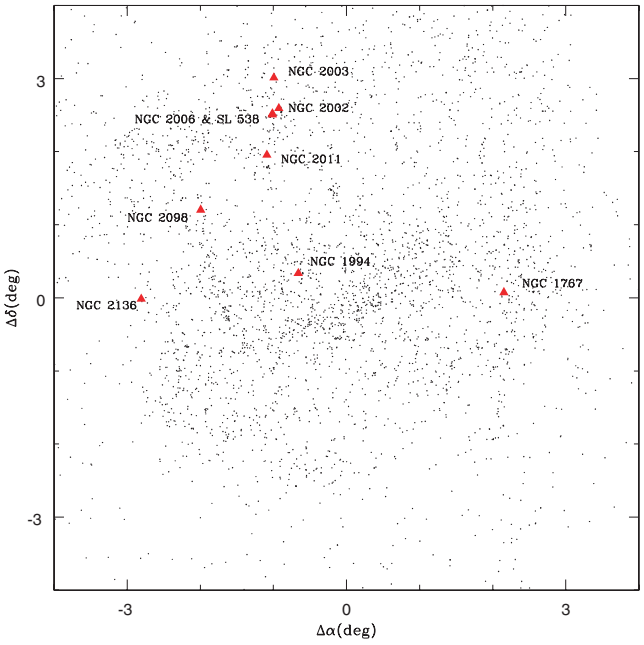

Figure 1. Small dots show the locations of identified LMC star clusters from the catalogue of Bica et al. (1999). A sky area of about $8^\circ \times 8^\circ$ is shown centred around the optical centre ($\alpha_{J2000} = 5^h20^m56^s$, $\delta_{J2000} = -69^\circ28'41''$) of the LMC. The bar region is clearly seen. The target clusters are shown with filled triangles.

1.1 Previous work

(i) **NGC 1767.** This cluster, a member of a triple star cluster system, is located in the OB association LH 8. Integrated $(U-B)$ and $(B-V)$ colours indicate that the cluster is young with an age of $\sim$10 Myr.

(ii) **NGC 1994.** This cluster, located in the LMC DEM 210 region, is a member of a five-cluster system. It has an irregular shape and is the largest of the five clusters. An age of about 5–30 Myr has been derived for the cluster from integrated photometric colour observations.

(iii) **NGC 2002.** This single cluster is located in the OB association LH 77 in the supergiant shell LMC 4 region. The cluster centre is condensed, but the outer part is resolved. Integrated light observations indicate an age of $\sim$10–30 Myr, along with the presence of a few red supergiants (Bica et al. 1996).

(iv) **NGC 2003.** Integrated photometric observations indicate an age of 10–30 Myr for this cluster, which is located in the Shapley III region of the LMC. Its shape on the photographic image is elongated with resolved outer parts.

(v) **NGC 2006 and SL 538.** This binary star cluster is located in the northwestern part of the OB association LH 77 in the supergiant shell LMC 4. The clusters are separated by $\sim$55 arcsec on the sky, corresponding to a linear separation of 13.3 pc at the distance of the LMC. Integrated photometric observations obtained by Bhatia (1992) and Bica et al. (1996) indicate similar ages for the two clusters. Using low-resolution objective prism spectra and integrated *IUE* spectra, Kontizas et al. (1998) suggested that this binary

cluster may merge in ∼10 Myr. Broad-band and Hα CCD photometric observations were obtained by Dieball & Grebel (1998). Based on the colour–magnitude diagrams (CMDs) of the clusters, they derived an age of 18 ± 2 Myr for SL 538 and of 22.5 ± 2.5 Myr for NGC 2006. The MF slopes obtained for both the clusters are consistent with that of Salpeter (1955) and indicate similar total masses. These studies thus indicate near-simultaneous formation of the cluster pair in the same giant molecular cloud.

(vi) **NGC 2011.** This cluster is located in the OB association region LH 75. Its age as estimated from the integrated photometric observations is between 10 and a few tens of millions of years. Its photographic image indicates that it is an elongated, fairly condensed and partly resolved cluster. A recent analysis of its stellar content using *HST* observations revealed that it has two parallel main-sequence branches, and may be a binary system (Gouliermis et al. 2006). However, the analysis also indicates that the two populations might have formed in a single star-forming event, as the redder stars are situated in the central half-arcmin region and are thought to be embedded in the dust and gas, whereas the blue stars are spread in the outer region up to distances of 1 arcmin.

(vii) **NGC 2098.** This is another single cluster. The first *BR* broad-band CCD photometric observations were presented by Kontizas et al. (1998). They derived an age of 63–79 Myr and found strong evidence for mass segregation, in agreement with their earlier studies based on the photographic observations. However, the poor quality of the CCD data was indicated by the authors.

(viii) **NGC 2136.** This is the brighter component of the young binary globular cluster NGC 2136/NGC 2137 in the LMC. The angular separation between the components is about 1.3 arcmin. Hilker, Richtler & Stein (1995), using Stromgren CCD photometry of the clusters, indicated their common origin. They gave an age of 80 Myr and a metallicity [Fe/H] of −0.55 ± 0.06 dex for the cluster, whereas Dirsch et al. (2000) derived an age of 100 ± 20 Myr but the same metallicity. The cluster contains a number of Cepheids as well as red giants.

Newly obtained CCD observations, in combination with earlier observations, have been used to estimate and/or interpret the interstellar reddening to the cluster regions, and the ages and MFs of the clusters. Section 2 deals with the observational data, reduction procedures and comparisons with the published photometric data. In Section 3, we analyse the stellar surface density profiles, CMDs and MFs of the sample clusters. The final section contains the results and discussions.

2 OBSERVATIONS AND DATA REDUCTIONS

The observations and procedures for data reduction are described in this section, along with the photometric accuracy and comparisons with published photometry.

2.1 Photometric data

The broad-band *BVRI* CCD photometric observations were carried out at the European Southern Observatory (ESO), La Silla, Chile, in 1990 between January 10 and 13 using the ESO Faint Object Spectrograph and Camera-2 (EFOSC-2) mounted at the Nasmyth focus of the 3.5-m New Technology Telescope (NTT). The filters used in these observations were standard Bessel BVR (ESO#583, 584, 585) and Gunn *i* (ESO#618). At the focus of the telescope, a 27-μm square pixel of the 512×512 size Tektronix CCD (#16) chip corresponds to ∼0.23 arcsec, and the entire chip covers a square area of side ∼2.0 arcmin on the sky. The read-out noise for the system was 14 e with a gain factor of 5.5 e/ADU. During our observations, the seeing varied from about 0.7 to 1.2 arcsec (see Table 2), with a mean value of 1.0 arcsec for the *B* band and of about 0.8 arcsec for the *V*, *R* and *I* bands. We obtained only one image for all clusters, as the CCD size was large enough to cover the entire region of the compact clusters. In the case of NGC 2002 and the binary cluster NGC 2136, we also imaged a field region located about 3 arcmin from the centre of the clusters. Table 2 lists the log of observations. Most of the observations were taken during the commissioning phase of the EFOSC2, when the instrument rotator was not yet available. As the image on NTT rotates during exposures at a rate that depends on the position on the sky, only exposures of up to at most a few minutes were possible. Bias frames were taken intermittently. Flat-field exposures were made of the twilight sky. Dark current frames were also secured.

Nine Landolt (1992) standards covering a range in brightness ($11.4 < V < 13.1$) as well as in colour ($-0.13 < (V - R) < 0.67$) were observed for calibration purposes. The excellent photometric

Table 2. Observing log of the CCD data taken for nine young LMC clusters during 1990. The suffix 'F' in the 'Object' column refers to the field region. The last column provides the number of stars (N) measured in various passbands. The seeing refers to the mean Gaussian FWHM of the stars.

Object	Date (Year 1990)	Band	Exp. (s)	Seeing (arcsec)	N
NGC 1767	Jan 10/11	*B*	20	1.05	632
		V	10	0.77	
		R	10	0.81	
NGC 1994	Jan 10/11	*B*	20	1.02	1156
		V	10,20	0.84	
		R	10,20×3	0.81	
		I	5	0.81	
NGC 2002	Jan 10/11	*B*	40	0.98	799
		V	20	0.72	
		R	15	0.88	
		I	10,20	0.86	
NGC 2002F	Jan 10/11	*B*	20	1.00	337
		V	10	0.84	
		R	10	0.72	
NGC 2003	Jan 10/11	*B*	60	0.81	729
		V	20	0.74	
		R	20	0.72	
		I	10	0.72	
NGC 2006	Jan 10/11	*B*	20	0.93	747
and		*V*	10	0.86	
SL 538		*R*	10	1.02	
	Jan 12/11	*B*	45	0.91	
		V	20, 30 × 2	1.00	
		R	8 × 2	0.88	
NGC 2011	Jan 10/11	*B*	60	0.91	610
		V	20	0.84	
		R	15	0.81	
NGC 2098	Jan 10/11	*B*	180	1.02	686
		V	60	0.86	
		R	15	0.81	
NGC 2136	Jan 12/13	*B*	60	1.00	1266
		V	30	0.93	
		R	15	0.86	
NGC 2136F	Jan 13/14	*B*	60	1.09	270
		V	30	0.88	
		R	15 × 2	0.86	

quality of the sky during the observations ensures the accuracy of the data presented here.

2.2 Reductions

The data were reduced using computing facilities available at the ARIES Observatory, Nainital. Initial processing of the data frames was done in the usual manner using the IRAF/MIDAS data reduction package. The flat-field frames were summed for each colour band. The evenness of flat fields is better than a few per cent in all the filters.

The magnitude estimate of a star on the data frames was performed using DAOPHOT software (Stetson 1987, 1992). Further processing and conversion of these raw instrumental magnitudes into the standard photometric system were performed using the procedure outlined by Stetson (1992). The image parameters and errors provided by DAOPHOT were used to reject poor measurements. About 10 per cent of the stars were rejected in this process. The DAOMASTER program was used to cross-identify the stars measured on different frames of a cluster region. For brighter stars that were saturated on deep-exposure frames, magnitudes were taken from the short-exposure frames. Most of the stars brighter than $V \sim 10.5$ mag could not be measured because they were saturated even on the shortest-exposure frames.

In deriving the colour equations for the CCD system and evaluating the zero-points for the data frames, we used mean values of atmospheric extinction coefficients of the site, namely 0.3, 0.2, 0.15 and 0.1 mag for the B, V, R and I bands, respectively. The colour equations for the CCD system were determined by performing aperture photometry on the photometric standards. By fitting least-square linear regressions in the observed aperture magnitudes as a function of the standard photometric indices, the following colour equations were derived for the system:

$$B - V = 1.219 \pm 0.024(b - v) - 1.113 \pm 0.028,$$

$$V - R = 1.065 \pm 0.019(v - r) - 0.116 \pm 0.016,$$

$$V - I = 1.062 \pm 0.010(v - i) + 1.101 \pm 0.014,$$

$$V - v = 0.032 \pm 0.017(V - R) - 1.145 \pm 0.013,$$

where B, V, R and I are the standard magnitudes provided by Landolt (1992). The terms B, V, R and i are the CCD aperture magnitudes. The rms deviations of the Landolt standards around the fitted magnitudes were found to be 0.033, 0.035, 0.027 and 0.026 mag for B, V, R and I, respectively. In order to establish the local standards, we selected about 30 isolated stars in each field and used the DAOGROW program to construct the aperture growth curve required for determining the difference between aperture and profile-fitting magnitudes. These differences, together with the differences in exposure times and atmospheric extinction, were used to evaluate zero-points for local standards in the data frames. The zero-points are uncertain by $\sim$0.013 mag in B, V, R and I.

The internal errors estimated from the scatter in the individual measures of different exposures in the NGC 2002 cluster region are listed in Table 3 as a function of magnitude for all filters. The errors become large ($\gtrsim$0.10 mag) for stars fainter than 20 mag. They can be considered as representative of the accuracy of our photometry in all the cluster and field regions under study. The numbers of stars measured in the various photometric passbands in an imaged region are given in Table 2. The X and Y pixel coordinates as well as V, $(B - V)$, $(V - R)$, and $(V - I)$ CCD magnitudes of the stars observed in the regions of NGC 1767, 1994, 2002, 2003, 2006, SL 538, NGC 2011, 2098 and 2136 are listed in Table 4. Stars observed by others are identified in the last column of the table. Only some of the results are presented here; the entire table is available in the electronic version of the article and also from the authors.

Table 3. Internal photometric errors in magnitude as a function of brightness in the NGC 2002 cluster region. σ is the standard deviation per observation in magnitude.

Magnitude range	σ_B	σ_V	σ_R	σ_I
$\leqslant$14.0	0.001	0.003	0.012	0.02
14.0–15.0	0.005	0.02	0.03	0.04
15.0–16.0	0.01	0.02	0.03	0.04
16.0–17.0	0.02	0.03	0.04	0.04
17.0–18.0	0.04	0.04	0.05	0.05
18.0–19.0	0.05	0.05	0.07	0.07
19.0–20.0	0.07	0.08	0.08	0.08

2.3 Photometric comparisons

We compare the newly obtained CCD photometric data with the published data for the clusters NGC 2006, SL538 and NGC 2098 in the following subsections.

(i) **NGC 2006 and SL 538.** The present photometry has 297 stars in common with the CCD photometric data given by Dieball & Grebel (1998). The plot of the differences between the two data sets (see Fig. 2) indicates that the present photometry is $\sim$0.04 mag brighter in V while the $B - V$ and $V - R$ colour agrees fairly well. The rms scatter in ΔV, $\Delta(B - V)$ and $\Delta(V - R)$ was found to be 0.08, 0.12 and 0.09 mag, respectively, and it can be understood in terms of the error present in both the photometries. There are a few outliers, which appear to be mostly stars located in the nucleus region of the cluster and which were treated as blended multiple stars in one of the photometries. We also note that the plot of differences with the colour show a small systematic trend in $\Delta(V - R)$, and it is apparent also to some extent in $\Delta(B - V)$. This may be caused by a second-order colour term from the B filter or by a minor calibration uncertainty present in one of the photometries.

(ii) **NGC 2098.** There are 174 stars in common between the present photometry and the BR data given by Kontizas et al. (1998). The differences between these data are plotted in Fig. 3. They indicate that there is a constant difference between the B and R magnitudes of the two data sets. We suspect that poor observing conditions during the Kontizas et al. (1998) observations may be responsible for the observed differences.

3 DATA ANALYSIS

The photometric data of the clusters under study were used to study the extent of the clusters along with their CMDs and MFs, as detailed in the following subsections.

3.1 Radial density profiles

The spatial surface density profile of stars can be used to determine the cluster radius, r_c, which is taken as the distance from the cluster centre to where the average cluster contribution becomes negligible with respect to the background stellar field. It can also be used to estimate the extent of field-star contamination in the cluster region.

Table 4. The relative positions (X, Y), CCD magnitude (V) and colours ($B-V$, $V-R$ and $V-I$) of all the stars measured in cluster and nearby field regions are presented sequentially for the clusters NGC 1767, 1994, 2002, 2002F, 2003, 2006 (including SL 538), 2011, 2098, 2136 and 2136F. Along with the star identification (ID), the cluster or field region identification is also provided in the first column. A sample is presented here; the full table is available in the online version of the article.

ID	X	Y	V	$B-V$	$V-R$	$V-I$
n1767_1	241.02	163.95	12.98 ± 0.01	0.22 ± 0.01	0.14 ± 0.01	–
n1767_2	251.32	91.73	13.04 ± 0.01	2.02 ± 0.01	1.02 ± 0.01	–
n1767_3	256.84	147.23	13.30 ± 0.01	1.91 ± 0.02	0.95 ± 0.01	–
n1767_4	60.10	34.90	13.46 ± 0.01	0.08 ± 0.01	0.12 ± 0.01	–
–	–	–	–	–	–	–
–	–	–	–	–	–	–

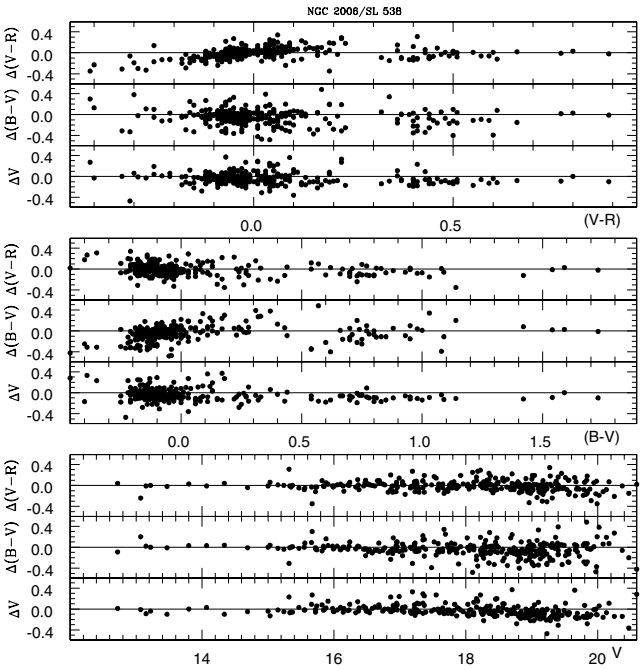

Figure 2. Comparison of the present photometry in NGC 2006/SL 538 with that of Dieball & Grebel (1998). The differences denote present minus literature data.

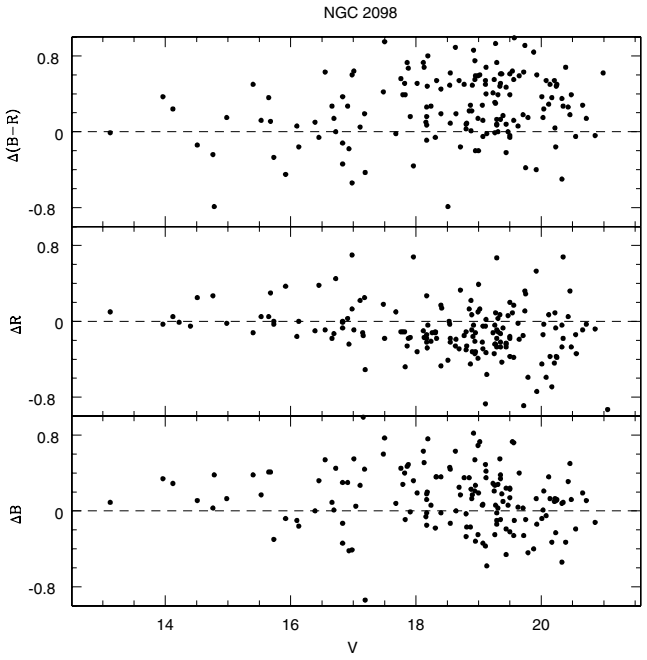

Figure 3. Comparison of the present photometry in NGC 2098 with that of Kontizas et al. (1998). The differences denote present minus literature data.

To do this, we first derive the cluster centre iteratively by calculating the average X and Y positions of stars within 150 pixel of an eye-estimated centre until they converge to constant values. An error of about 10 to 20 pixel is expected in locating the cluster centre. The (X,Y) pixel coordinates of the cluster centres are given in Table 5. In order to determine the radial surface density of stars in a cluster, the imaged area was divided into a number of concentric circles with respect to the above-estimated cluster centre, in such a way that each zone contains a statistically significant numbers of stars. The number density of stars, ρ_i, in the ith zone is evaluated as

$$\rho_i = \frac{N_i}{A_i},$$

where N_i is the number of stars up to $V \sim 20$ mag and A_i is the area of the ith zone. Wherever the zones cover only part of the imaged cluster area, the area of the zone has been accounted for in the determination of A_i. The assumed concentric circles and the stellar surface densities derived in this way for the clusters under discussion are shown in Figs 4 to 13. The presence of a clear radius–density variation confirms the relatively small diameters (compactness) of the star clusters under study.

Table 5. Estimated coordinates of the cluster centre (X_c, Y_c), cluster radius (r_c) and the radius limits of the regions. All the units are in pixels, and one pixel corresponds to ∼0.23 arcsec on the sky.

Cluster	X_c	Y_c	r_c	Core	Ring 1	Ring 2
NGC 1767	255	355	150	$r < 30$	$30 \leqslant r < 80$	$80 \leqslant r < 150$
NGC 1994	240	275	240	$r < 30$	$30 \leqslant r < 80$	$80 \leqslant r < 240$
NGC 2002	250	280	240	$r < 30$	$30 \leqslant r < 80$	$80 \leqslant r < 240$
NGC 2003	265	240	220	$r < 15$	$15 \leqslant r < 65$	$65 \leqslant r < 220$
NGC 2006	285	90	120	$r < 10$	$10 \leqslant r < 60$	$60 \leqslant r < 120$
SL 538	230	310	110	$r < 20$	$20 \leqslant r < 60$	$60 \leqslant r < 110$
NGC 2011	240	245	220	$r < 30$	$30 \leqslant r < 75$	$75 \leqslant r < 220$
NGC 2098	260	250	160	$r < 25$	$25 \leqslant r < 80$	$80 \leqslant r < 160$
NGC 2136	280	275	260	$r < 35$	$35 \leqslant r < 90$	$90 \leqslant r < 260$

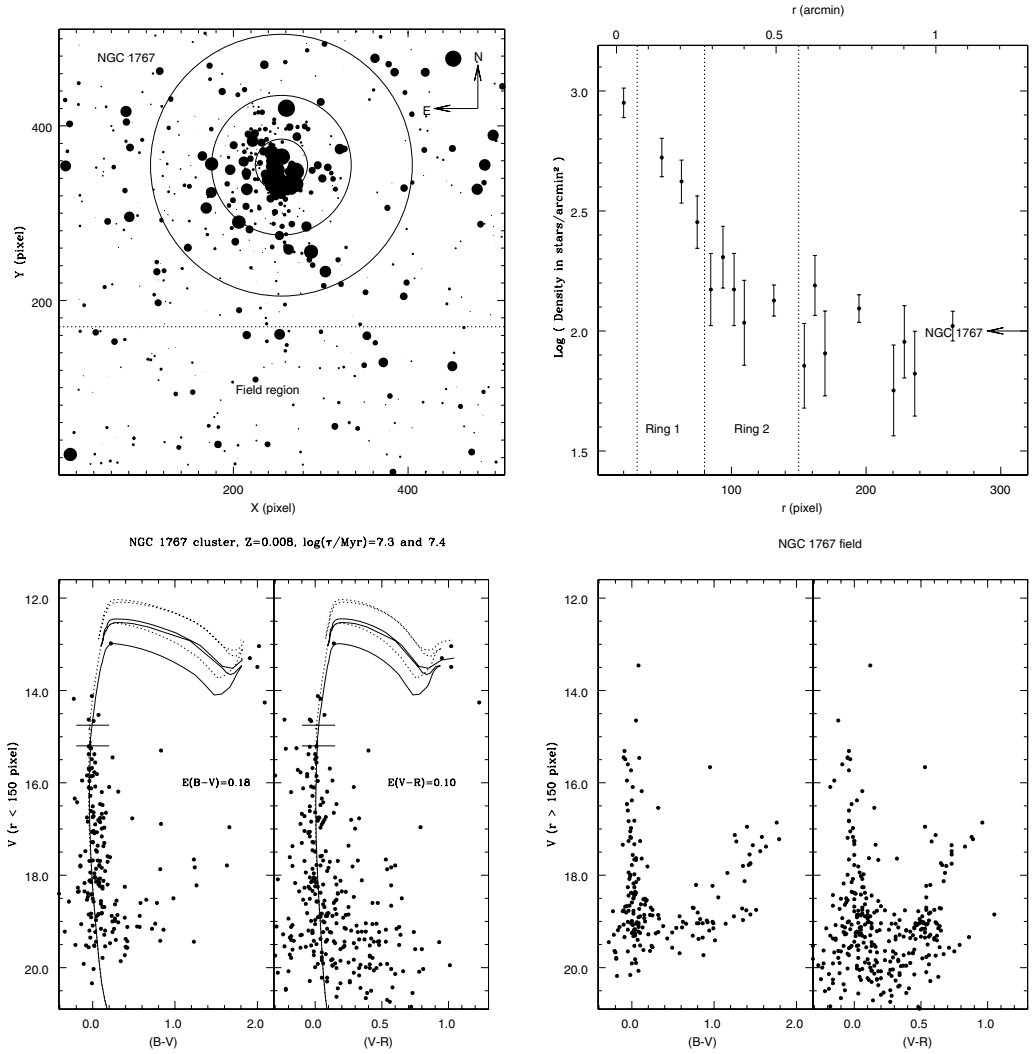

Figure 4. NGC 1767. (a) Identification chart for the observed $\sim 2 \times 2$ arcmin^2 region of NGC 1767 by EFOSC2/NTT. The sizes of the filled circles are proportional to the apparent magnitude in such a way that brighter stars have larger sizes. North is up and east is to the left. The innermost ring defines the core region, and the outermost ring represents the cluster boundary (see Table 5). Except for NGC 2002 and NGC 2136, the field region is considered beyond the outermost ring. (b) Stellar surface density of stars around the cluster centre. Poisson errors are shown with vertical bars. The first and third dotted vertical lines represent the core and cluster radius, respectively. The Ring 1 and Ring 2 regions are used for mass function determination. The horizontal arrow at the rightmost corner of the plot shows the field-star density. (c) The CMDs for the cluster region ($r < r_c$). The two isochrones from Girardi et al. (2002) confining the best age estimates are shown by dotted (younger ishochrone) and solid (older isochrone) continuous curves. An LMC distance modulus of 18.5 and normal reddening law have been assumed. The resulting colour excess parameters are given in the respective CMD panel. The main-sequence gaps (see Table 6) are marked with horizontal bars. (d) The CMDs for the field region alone ($r > r_c$). The reduced stellar density for the main-sequence as well as the red clump around $(V - R) \sim 0.5$ mag, $(B - V) \sim 0.95$ mag and $V \sim 19.5$ mag are clearly seen.

The level of field-star density derived from the outer region is also shown in these figures. The field-star densities up to $V = 20$ mag are in the range of 69 to 102 stars arcmin^{-2}, with an average value of about 80 stars arcmin^{-2}. For NGC 2002 and 2136, the field-star density is also estimated from a 2 arcmin $\times$ 2 arcmin region lying $\sim$3 arcmin from the cluster centre. The derived mean densities are 78 and 56 stars arcmin^{-2}, respectively. The corresponding values derived from the outermost region of the clusters ($r > r_c$) are 79 and 80 stars arcmin^{-2}. Within our statistical uncertainty, they are similar. It can therefore be concluded that the extent of field-star contamination is similar in all the clusters under discussion. We also derive the spatial variation of the field-star density from the imaged field regions, taking $X = 256$ pixel and $Y = 256$ pixel as its centre, and these variations are shown in Figs 6 and 12. It is seen that the stellar density of the field region follows the background densities derived from the outermost regions of these two clusters. This indicates that stars with $r > r_c$ can be used to estimate field-star contamination in the cluster. From these numbers as well as from the cluster sequences present in the colour–magnitude diagrams discussed below, it can be said that the field-star contamination in stars brighter than $V \sim 20$ mag is not strong enough to smear the cluster sequences, and hence does not affect the results derived below.

As a large fraction of our data are incomplete in the crowded central region of the clusters, we are unable to evaluate the value of the stellar density at the cluster centre. Consequently, the radius at which the central stellar density is halved cannot be determined. However, the radial density profiles of all the clusters clearly indicate

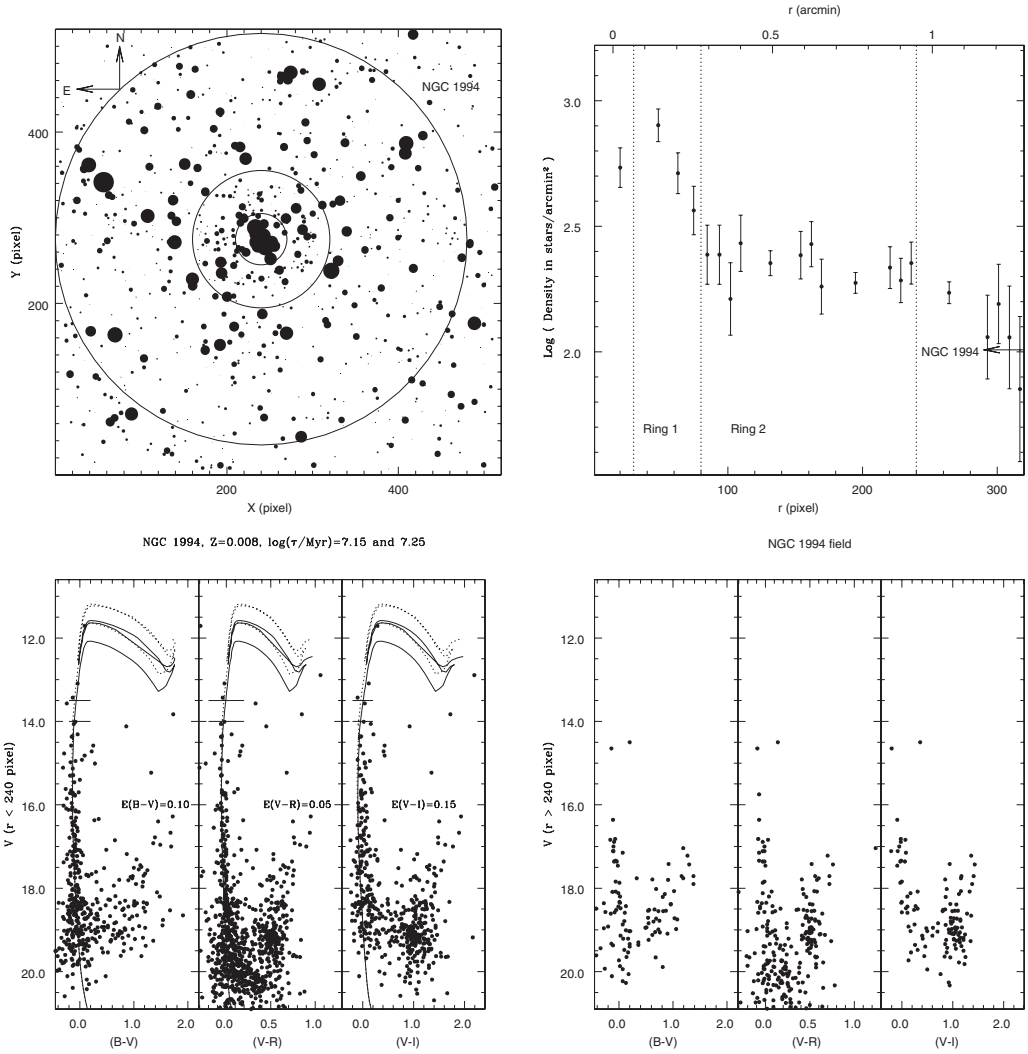

Figure 5. As Fig. 4, but for NGC 1994.

the innermost cluster region ($\leqslant$30 pixel) in which stellar crowding is so great that it cannot be used to determine the cluster MF accurately. Similarly, the outermost regions of the clusters where the stellar density becomes flat is clearly defined, and we have considered this as the cluster radius. In Figs 4 to 6 and 8 to 12, it can be seen that, for all the clusters, beyond a radius $R \sim 0.9$ arcmin the number of starsup to 20 mag per unit area drops to a uniform level, which might be considered as a good approximation of the background density. The cluster radius for the target clusters ranges from 120 pixels ($\sim$0.5 arcmin) for NGC 2006 and SL 538 to 260 pixels ($\sim$1.0 arcmin) for NGC 2136. Its value is about 0.75 arcmin for NGC 1767 and 2098, and the other clusters have a radius of about 0.92 arcmin. In order to see radial variations of the MF, the entire cluster region (excluding the core) has been divided into two annulus region, namely Ring 1 and Ring 2. The pixel values of the cluster radius, core region, Ring 1 and Ring 2 are listed in Table 5.

3.2 Colour–magnitude diagrams

In order to analyse the CMDs of our LMC clusters properly, it is necessary to delineate the cluster sequences from the unavoidable field-star contamination. We therefore constructed CMDs of stars located at different radial distances from the cluster centre. This helps us to distinguish cluster features from features characterizing the surrounding LMC fields. Consequently, two CMDs for each cluster, one representing the features of the cluster and the other characterizing the surrounding field region, were constructed. Figs 4 to 6 and 8 to 12 show the CMDs of the cluster ($r \leqslant r_c$) as well as of the field ($r > r_c$) regions. For NGC 2002 and 2136, we also show the CMDs of nearby field (2 arcmin $\times$ 2 arcmin) regions in Figs 7 and 13, respectively. A characteristic main-sequence (MS) from $V \sim 14$ to 20 mag is seen in all the clusters, except for NGC 2136 for which it begins at around $V \sim 16$ mag, indicating their youthful (age $\lesssim$25 Myr) nature. In addition, the brighter ends ($V \sim 13$ mag) are also populated by a few blue and red supergiants. This is in contrast to the field regions, which are only sparsely populated by stars towards the lower MS ($V \gtrsim 16$ mag). Red clumps of stars near $V \sim 19.5$ mag, $(B - V) \sim 0.9$ mag and $(V - R) \sim 0.5$ mag in the CMDs are populated by evolved stars arising from the old-age ($\gtrsim$1 Gyr) stellar populations of the LMC. Such a feature has also been observed in other CCD photometric studies of LMC star clusters (see Sagar, Richtler & de Boer 1991, and references therein). These are core helium-burning stars of the LMC field forming a clump in the CMDs.

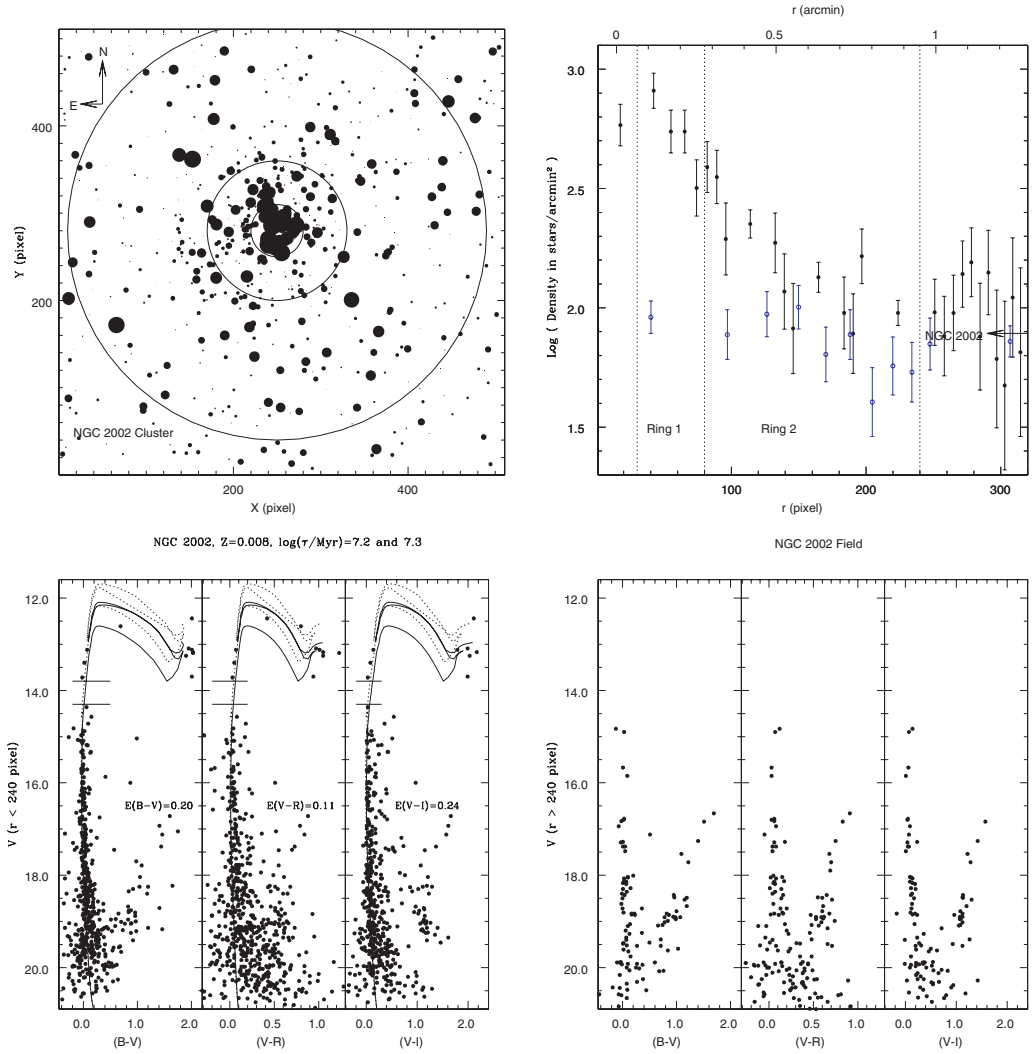

Figure 6. As Fig. 4, but for NGC 2002. Part (b) also shows the radial star density (open circles) of the field region imaged about 3 arcmin from the cluster centre and shown in Fig. 7; the centre is selected arbitrarily at $X = 256$ and $Y = 256$ pixel.

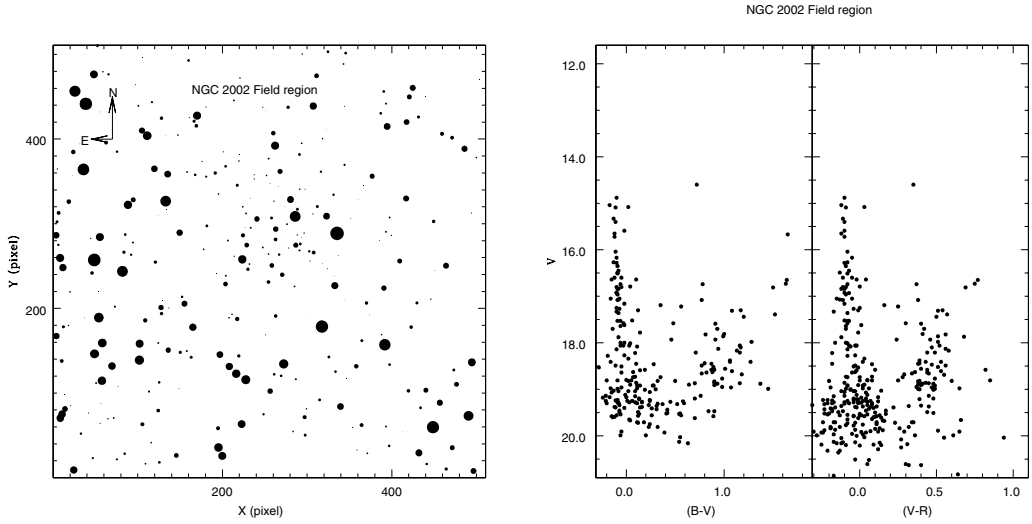

Figure 7. Identification chart and CMDs for the NGC 2002 field region.

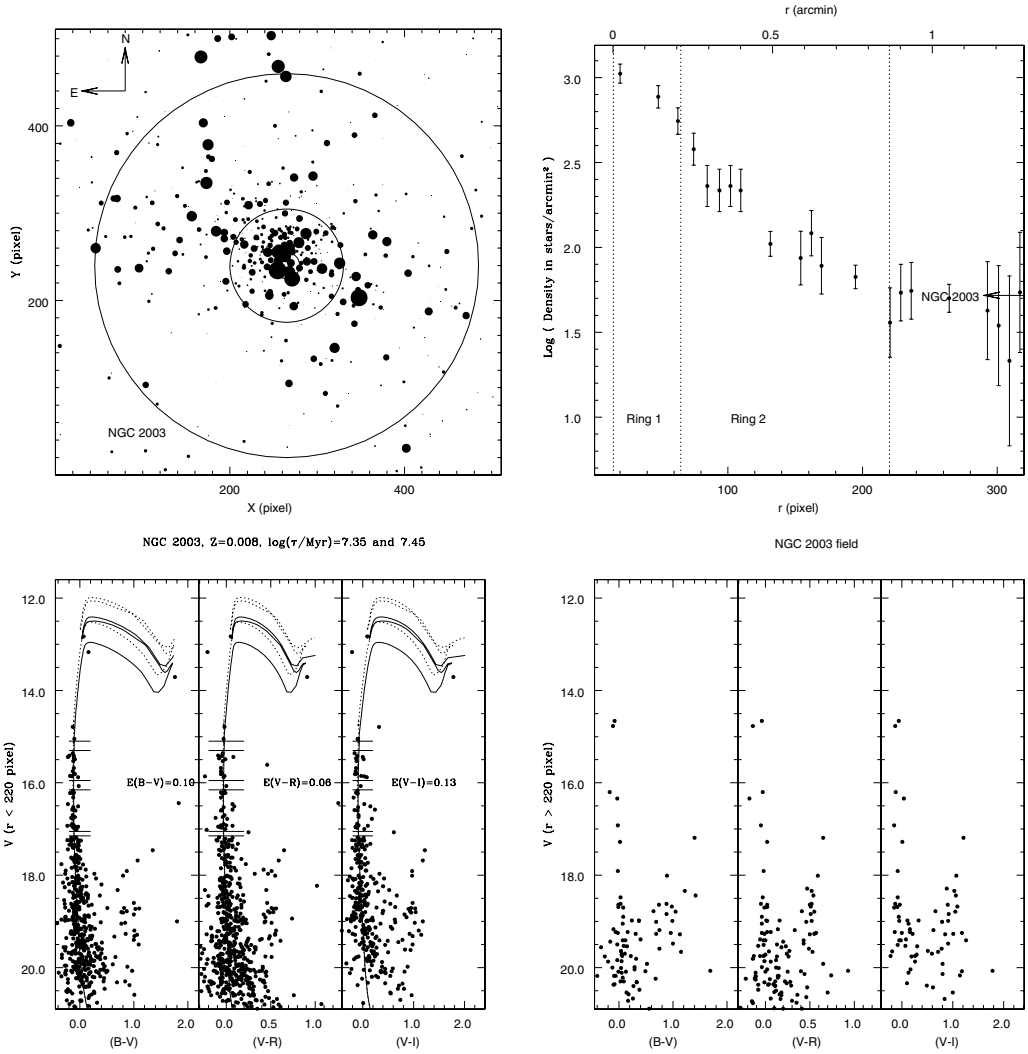

Figure 8. As Fig. 4, but for NGC 2003.

In order to construct mass functions of the clusters under study, we need to determine the distance, age and reddening for each object, and these are described below.

The value of 18.5 ± 0.1 mag for the true distance modulus of the LMC is now well constrained as it is derived using more than two dozen independent measurements (see Alves 2004; Schaefer 2008, and references therein). The individual determinations, however, vary from 18.1 to 18.8 mag, primarily owing to the use of different standard candles, for example the Red clump, tip of the red giant branch, Cepheids, RR Lyrae stars, Mira variables, SN1987A, eclipsing binaries, etc. We adopt 18.5 ± 0.1 mag as the distance modulus for the LMC in the present study. As colour excess, reddening law and metallicity are similar, smaller distances result in lower ages and affect the derived mass ranges for MFs. A closer analysis indicates that adopting a change in the distance modulus of 0.4 mag changes the derived MFs significantly, although its effect on MF slopes is observed to be negligible (Sagar & Richtler 1991).

We use the stellar evolutionary models by Girardi et al. (2002) to estimate cluster ages, and adopt a constant value of metallicity of $Z = 0.008$ (Fe/H ~ 0.3 dex). Recent estimates on the present-day chemical abundance for LMC stellar population converge to a sub-solar metallicity; for example, Rolleston, Trundle & Dufton (2002) derive a metallicity index of -0.31 ± 0.4 for OB-type MS stars. For many young ($\tau < 100$ Myr) LMC star clusters, the metallicity seems to have a plateau at around Fe/H ~ 0.4. (Mackey & Gilmore 2003; Kerber, Santiago & Brocato 2007). The effects of metallicity variation on the derived MF slope indicate that it becomes flatter with decreasing values of Z. A change in Z from 0.02 to 0.004 has a negligible effect on the MF slope – see fig. 6 of Sagar & Richtler (1991).

Reddening towards the surrounding LMC region is observed to be around $E(B - V) = 0.075$ mag as estimated from all sky maps at 100 μm (Schlegel, Finkbeiner & Davis 1998). Based on an H I emission map (Burstein & Heiles 1982), the predicted values of $E(B - V)$ towards the clusters lie between 0.05 and 0.1 mag. However, the intragalactic reddening across the LMC is observed to vary and it may be as high as 0.3 mag in some regions (Bessell 1991). We therefore adjusted the value of reddening to best fit the isochrones to the MS. Our age estimates are greatly facilitated by the presence of a few blue and red supergiants. The best estimate for age lies between two isochrones identified for each cluster and shown in Figs 4 to 6 and 8 to 12, and accordingly we adopt a mean age (τ/Myr) and uncertainty. The reddening and the adopted ages derived in this way are listed in Table 6. The value of $E(B - V)$ is $\leqslant 0.1$ mag for all

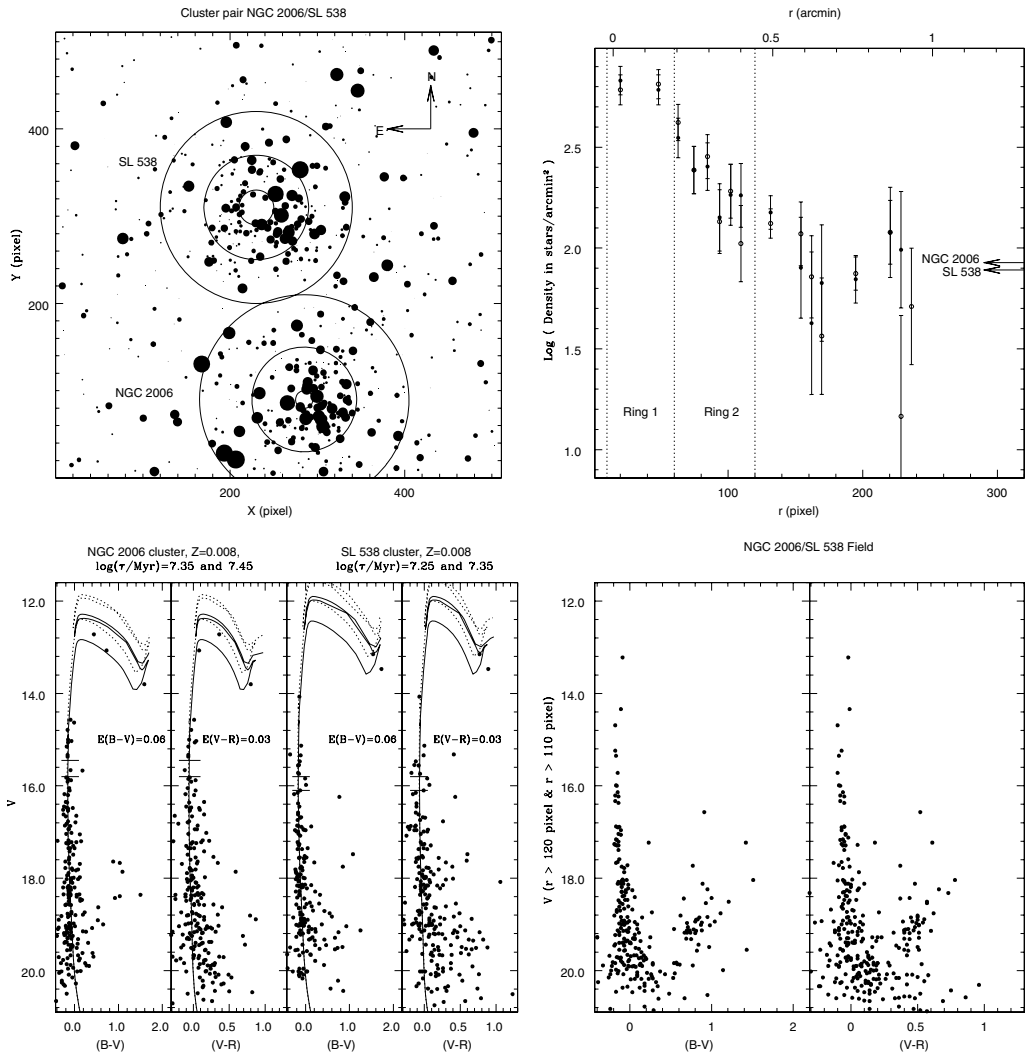

Figure 9. NGC 2006 and SL 538. The two left panels in (c) correspond to NGC 2006 and the stars are shown with $r < 120$ pixel, and the two right panels correspond to SL 538 with $r < 110$ pixel. Other descriptions are as in Fig. 4.

the clusters except NGC 1767 and 2002, for which it is 0.18 and 0.2 mag, respectively. Thus the low reddening values found here are in agreement with those based on H I and dust emission maps of sky.

The age estimates for NGC 2006 (25 ± 3 Myr) and SL 538 (20 ± 2 Myr) are consistent with the corresponding estimates of 22.5 ± 2.5 Myr and 18 ± 2 Myr by Dieball & Grebel (1998). Our age estimate (32 ± 4 Myr) for NGC 2098 is significantly younger than the estimate of 63–79 Myr by Kontizas et al. (1998). For all other clusters, the estimates derived here are the first reliable estimate of age using the MS turn-off point in the CMDs. However, studies using integrated spectra of star clusters and single-population stellar libraries derive ages that are systematically about 10 Myr younger (Wolf et al. 2007). Barring NGC 2098 and 2136, Wolf et al.'s (2007) age estimates for the remaining seven clusters of our sample lie between 6 and 8 Myr, whereas our estimates range from 15 to 20 Myr. The age estimates derived from integrated spectra using theoretical models seem to be biased towards blue MS stars.

A gap in the MS is defined as a band, not necessarily perpendicular to the MS, with no or very few stars. Böhm-Vitense & Canterna (1974) first located a gap in the MS around $(B - V)_0 = 0.27$ mag, which arises as a result of the onset of convection in the stellar envelope. Gaps seem to appear as statistically distinct features in the MS of star clusters (Sagar & Joshi 1978; Kjeldsen & Frandsen 1991; Subramaniam & Sagar 1999). MS gaps in the present sample were identified visually, and the gap parameters are listed in Table 6. Except for NGC 2136, all the target clusters have a gap of about 0.3 to 0.5 mag width between $M_V \sim -3.0$ and -5.0 mag. This seems to be a characteristic feature of stellar evolution, as the brighter gap location corresponds to the younger clusters. Stellar evolution models do predict a paucity of stars around and beyond the MS turn-off. However, some clusters seem to have a clumpy MS with more than one gap; for example, NGC 2003 and 2011 show gaps of smaller amplitude ($\Delta V < 0.3$ mag) at fainter magnitudes. Both these clusters have elongated spatial structures and may have a star-forming history different from that of the other clusters. It is therefore noted that the gaps may also arise as a result of stochastic effects of star formation and sampling along the MS, and may not represent a genuine astrophysical effect.

3.3 Cluster luminosity and mass functions

The luminosity functions (LFs) of LMC star clusters and their corresponding field regions are derived from star counts in a bin width of 0.5 mag in V from the V, $(V - R)$ diagram. This diagram is

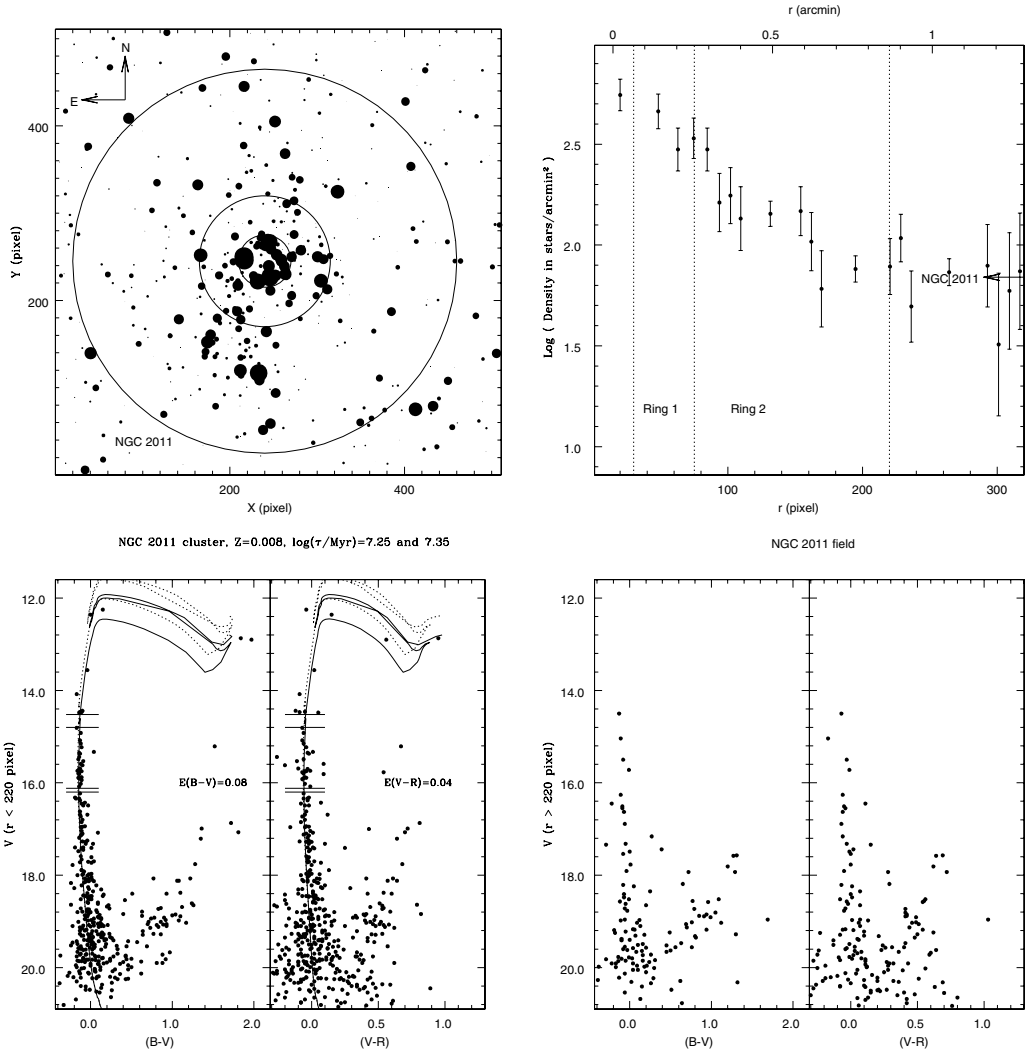

Figure 10. As Fig. 4, but for NGC 2011.

preferred over other CMDs because of the fainter limiting magnitude and better data completeness. The main factors that limit the precise determinations of the cluster MF from the present observations are data incompleteness and field-star contamination: the central regions of the clusters are more likely to suffer from data incompleteness, whereas the outer regions are more affected by field-star contamination. Moreover, the present photometry is generally not able to resolve the central 30-pixel-diameter region of each cluster. We therefore, estimate the LFs for the inner (Ring 1), outer (Ring 2), and entire regions of each cluster excluding the core. These regions are marked in the radial density profile of the respective clusters (see Section 3.1) and are listed in Table 5.

For the data completeness factor (CF), we follow the usual DAOPHOT procedure of adding and recovering artificially selected stars with known magnitudes and positions in the original V and R frame, and the effective CF is taken to be the smaller value of V and R. We estimate the CF separately for the inner, outer, and entire regions as well as for the corresponding field region, which is usually defined as $r \geqslant r_c$ (see Table 5). In the case of NGC 2002 and 2136, the field region refers to the full CCD frames of a nearby field. For each region, the number of stars (NS) lying on the MS in the V, $(V - R)$ diagram is counted in a bin width of 0.5 mag. In order to avoid field-star contamination from intermediate-age stellar populations of the LMC, which normally appear as a characteristic red clump near $V \sim 19.5$ mag and $(V - R) \sim 0.5$ mag, the stars are counted in a 0.5-mag strip around the best-fitting isochrones. The LF for each bin is calculated as

$$\mathrm{LF} = \left(\frac{\mathrm{NS}}{\mathrm{CF}}\right)_{\mathrm{cluster}} - \left(\frac{\mathrm{NS}}{\mathrm{CF}}\right)_{\mathrm{field}} \times \text{area factor}.$$

We present the derived LFs for all the clusters in Table 7. Column 1 provides the magnitude bin, and columns 3 to 10 provide CF and NS values for the inner, outer, entire and field regions, respectively. The LFs corrected for the data incompleteness and the field-star contamination (corrected for the area difference between the cluster and field region) are given in the last three columns, and the masses corresponding to the centre of the magnitude bin derived from the best-fitting isochrones (see Section 3.2) are given in the second column. For the outer region of NGC 2098, the MF could not be derived owing to poor statistics.

4 RESULTS AND DISCUSSIONS

To convert the LFs into MFs, we divide the number given in Table 7 by the mass interval, ΔM, of the magnitude bin under consideration. The value of ΔM is obtained from the mass–luminosity relation

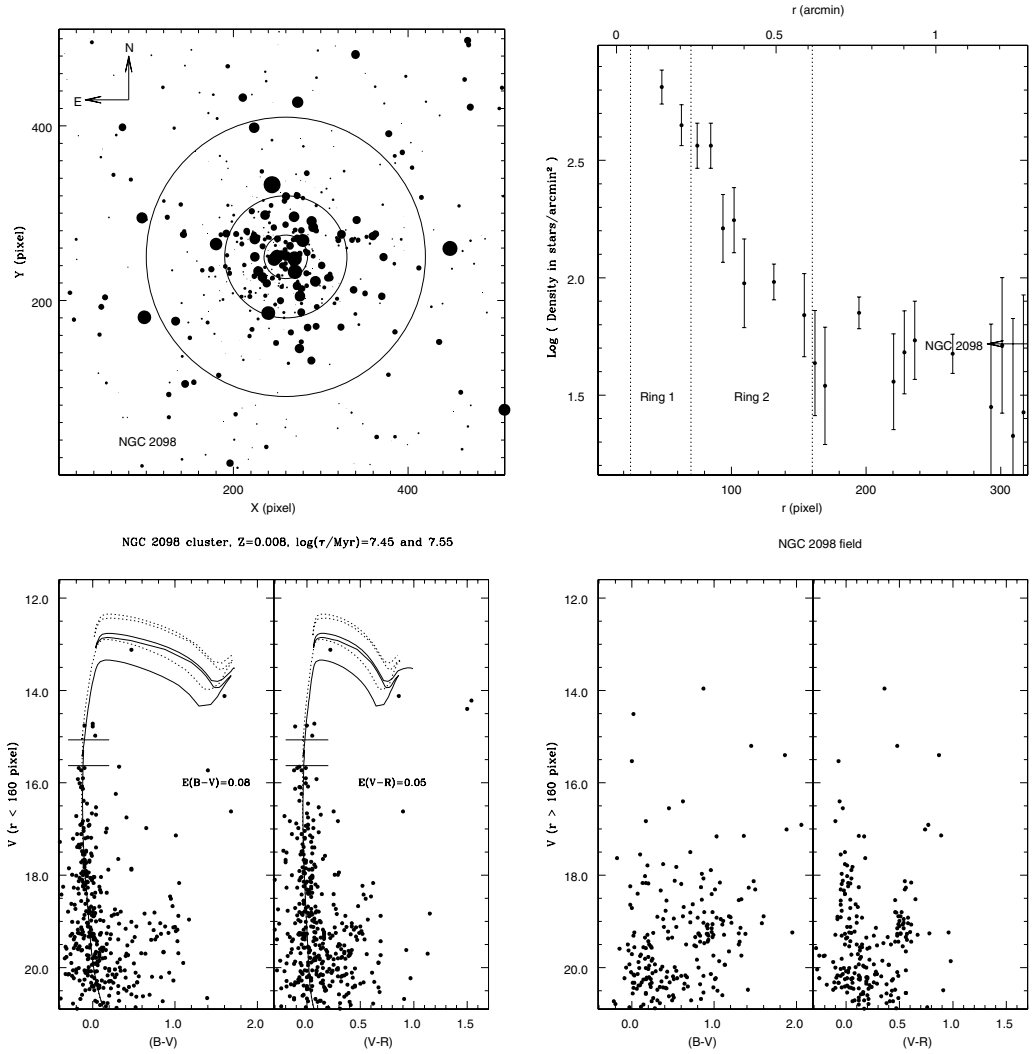

Figure 11. As Fig. 4, but for NGC 2098.

derived from the appropriate isochrones. The resulting cluster MFs are plotted in Fig. 14 and the slopes are given in Table 6. The quoted uncertainties result from the linear regression solution. The slope is derived from the mass distribution function $\xi(M)$, which is assumed to be a power law with index γ. If dN denotes the number of stars in a bin with central mass M, the value of γ is determined from the linear relation

$$\log(\mathrm{d}N) = \gamma\ \log(M) + \text{constant}.$$

γ is also denoted as $-(1 + x)$ in the literature, with $\gamma = -2.35$, or $x = 1.35$ being the Salpeter (1955) value.

For NGC 2002, 2006, 2011 and 2136, the MF slopes for the inner (Ring 1) and outer (Ring 2) cluster regions differ by about 1 dex and are shallower for the inner cluster region. In the case of NGC 2098, too, the MF slope for the entire region is steeper than that for the inner region. However, because of poor statistics, the MF slope for the outer region could not be derived. Kontizas et al. (1998) found a similar trend for SL 566 and NGC 2098; that is, shallower LF slopes in the inner regions of the clusters. This could be interpreted as mass segregation (high concentration of heavier stars in the central region) and may arise as a result of star formation or dynamical evolution processes. As the ages of the clusters under discussion are less than the dynamical relaxation time, the observed variation may be an imprint of star formation. However, we note that the combined effect of scatter in the MF slope may be as large as 1 dex, and, hence, we suggest using *HST* observations to resolve the stars of the cluster core region and to confirm the radial variation of the MF slope. In the remainder of the discussion, we consider only the MF slope derived for the total cluster region.

The mass ranges for the sample clusters are similar, namely ∼2 to 12 $M_\odot$, except for NGC 2136, for which it is only 2 to 6 $M_\odot$. As the ages of all the clusters are less than the dynamical evolution times (∼100 Myr), the slopes of the present-day MFs can be considered as the slopes of the IMFs. Furthermore, we also assume that all the stars in the cluster are formed in a single star-forming burst, and hence if the most evolved stars, e.g. supergiants, were left out, the derived MFs could be least affected by the star formation history of the clusters. Excluding NGC 1767, we obtain a mean MF slope of -2.13 ± 0.14 for eight target clusters. This value is not too different from the Salpeter value derived for solar neighbourhood stars and for other young galactic and M33 star clusters in the intermediate-mass range (cf. Sagar 2000, 2002; Chen, De Grijs & Zhao 2007).

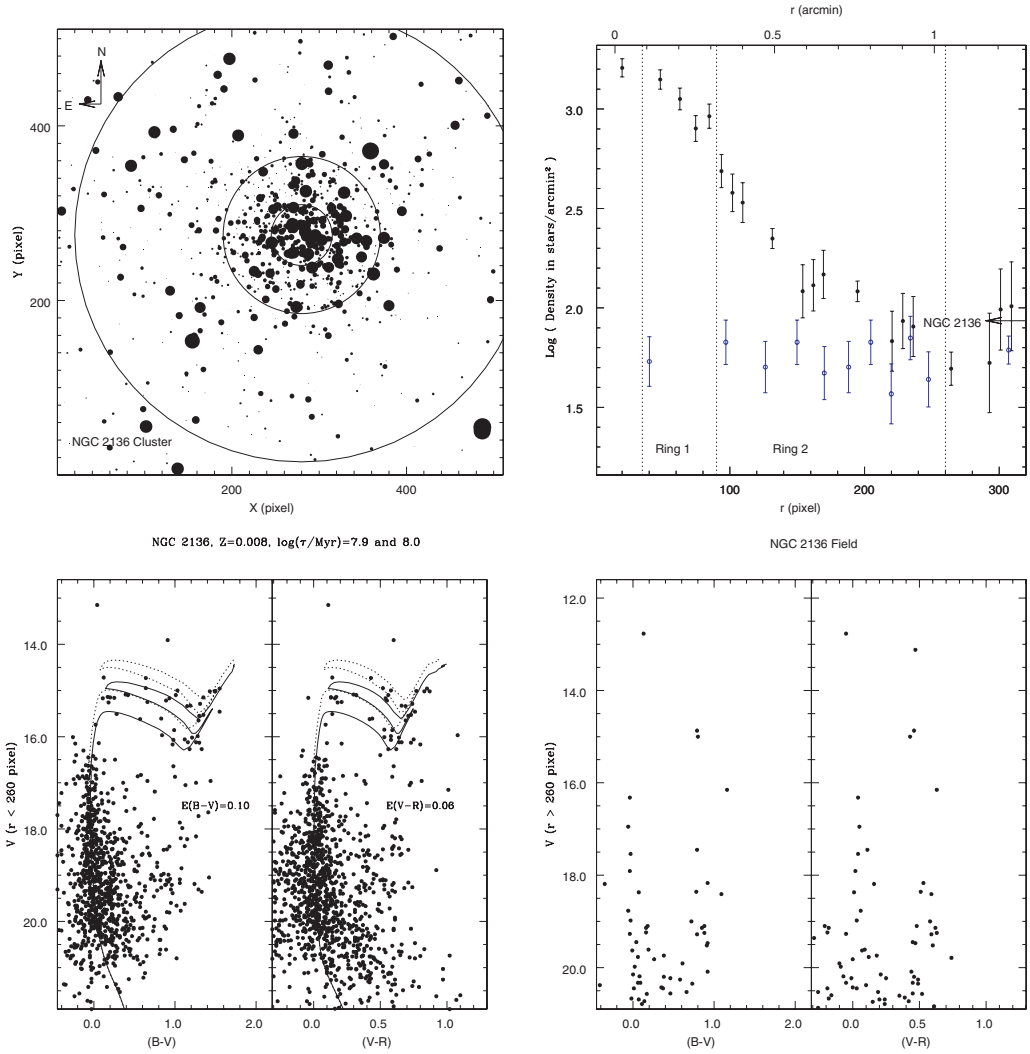

Figure 12. As Fig. 4, but for NGC 2136. Part (b) also shows the radial star density (open circles) of the field region imaged about 3 arcmin from the cluster centre and shown in Fig. 13; the centre is selected arbitrarily at $X = 256$ and $Y = 256$.

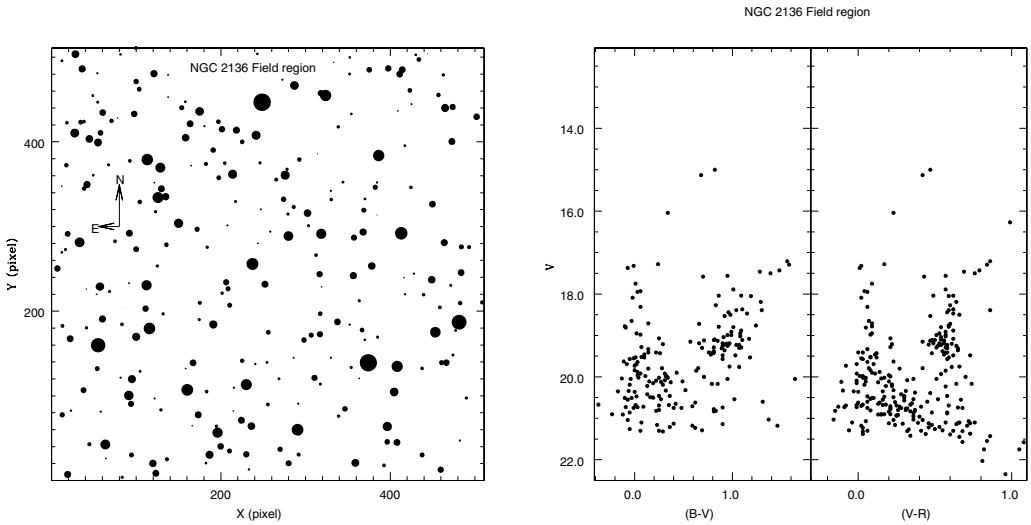

Figure 13. Identification chart and CMDs for the NGC 2136 field region.

Table 6. Derived reddening, $E(B-V)$, and age parameters from the CMDs are listed in the second and third columns for the sample clusters. MS gap parameters, for example location magnitude (V_0), gap width (ΔV_0) and colour ($(B-V)_0$) are given in columns 4 to 6. The MF slopes for the 'Ring 1', 'Ring 2' and 'Total' cluster region are listed in the remaining columns. MF slopes were derived using the V, $(V-R)$ diagrams.

Cluster	$E(B-V)$	Age	MS gap parameters			MF slopes		
	(mag)	(Myr)	V_0	ΔV_0	$B-V_0$	Ring 1	Ring 2	Total
NGC 1767	0.18	23 ± 3	-4.14	0.45	-0.20	-1.46 ± 0.36	-1.39 ± 0.54	-1.23 ± 0.27
NGC 1994	0.10	16 ± 2	-5.08	0.50	-0.18	-2.56 ± 0.36	-2.00 ± 0.52	-2.15 ± 0.31
NGC 2002	0.20	18 ± 2	-5.07	0.50	-0.20	-1.73 ± 0.43	-2.50 ± 0.20	-2.28 ± 0.21
NGC 2003	0.10	25 ± 3	-3.61	0.20	-0.22	-2.37 ± 0.24	-2.28 ± 0.21	-2.22 ± 0.18
			-2.76	0.20	-0.23			
			-1.69	0.15	-0.21			
NGC 2006	0.06	25 ± 3	-3.07	0.35	-0.23	-1.25 ± 0.16	-2.62 ± 0.53	-1.90 ± 0.16
SL 538	0.06	20 ± 2	-2.74	0.30	-0.23	-2.33 ± 0.32	-1.82 ± 0.68	-2.03 ± 0.41
NGC 2011	0.08	20 ± 2	-4.08	0.28	-0.21	-1.72 ± 0.54	-2.41 ± 0.43	-2.01 ± 0.50
			-2.59	0.08	-0.22			
NGC 2098	0.08	32 ± 4	-3.39	0.56	-0.19	-1.73 ± 0.13	–	-2.19 ± 0.19
NGC 2136	0.10	90 ± 10	-	-	-	-2.13 ± 0.39	-3.00 ± 0.49	-2.22 ± 0.20

The MF slope for NGC 1767 was found to be significantly flatter ($\gamma \sim -1.23$) than the Salpeter value.

Our MF slopes of -1.90 ± 0.16 for NGC 2006 and of -2.03 ± 0.41 for SL 538 are consistent with the corresponding values of 2.27 ± 0.32 and -2.22 ± 0.31 derived by Dieball & Grebel (1998). Fig. 15 shows the variation of MF slope with galactocentric distance for 26 young (<100 Myr) star clusters and associations in the LMC. The figure includes nine clusters from the present work, and data for other objects taken from table 1 of Sagar (2000). For four clusters, we have two estimates for the MF slope, and these points are all shown in Fig. 15. Treating NGC 1767 as an outlier, the remaining sample of 25 has a mean MF slope $\gamma = -2.22 \pm 0.16$, indicating that the MF slope in LMC clusters is not significantly different from the Salpeter (1955) value. The scatter seen in Fig. 15 in MF slope is caused by many factors, for example data incompleteness and field-star contamination, the dynamical and stellar evolutionary state of the star clusters, the limited range in mass, the model assumed to derive the mass–luminosity relation, and the Poisson noise (Kroupa 2001; Sagar & Richtler 1991; Sagar 2002). Detailed analysis indicates that the cumulative effect of the various uncertainties could be as large as 0.4 dex for young rich LMC star clusters (Sagar 2002). We therefore conclude that the scatter seen in Fig. 15 is real and does indicate the limitations of MF slope determinations from ground-based observations. Despite being situated in different locations of the LMC, the studied sample of young clusters and associations supports the idea of some universal IMF as a consequence of star formation processes in star clusters and associations.

5 SUMMARY

We present *BVRI* CCD data obtained from 3.5-m ESO NTT/EFOSC2 observations for nine young LMC star clusters, namely NGC 1767, 1994, 2002, 2003, 2006, SL 538, NGC 2011, 2098 and 2136, and their nearby field regions reaching down to $V \sim 20$ mag for ~ 6400 stars altogether. The data represent the first accurate broad-band CCD photometric data for all the clusters, except for the binary cluster NGC 2006 and SL 538. The observations were made in a region of $\sim$2 arcmin$\times$ 2 arcmin around the cluster centre. The data were collected during 1990 January 10 to January 13, in good seeing conditions ranging from 0.7 to 1.0 arcsec, and were reduced using DAOPHOT and MIDAS software. Photometric calibrations were performed using Landolt (1992) stars, and the zero-point accuracy is better than 0.02 mag. Photometric errors become large ($\gtrsim$0.1 mag) for stars fainter than $V = 20$ mag.

We examined radial density profiles and general features of the main sequence, and estimated age and reddening for individual clusters using Padova isochrones. The various CMDs of the clusters under study were used to estimate their MF, age and reddening. In order to study radial variation in the MF, the LFs were derived for inner, outer, and entire cluster regions. Owing to the compactness of the clusters, such study could not be carried out for the core regions of the clusters. The LFs were corrected for both data incompleteness and field contamination. The main conclusions of the study are as follows.

(i) Seven of the nine clusters have ages $\leqslant$25 Myr, and the remaining two clusters have ages of 32 ± 4 Myr (NGC 2098) and 90 ± 10 Myr (NGC 2136). Our age estimates for NGC 2006 and SL 538 are consistent with the previous *BVR* photometric estimate by Dieball & Grebel (1998). For NGC 2098, our estimates are lower by about 30 Myr than those of Kontizas et al. (1998). Thus, the ages of all the clusters in our sample are significantly lower than their typical dynamical ages of a few hundred million years.

(ii) For younger ($\leqslant$25 Myr) clusters, the age estimates based on a recent population synthesis model by Wolf et al. (2007) and integrated spectra are systematically lower by about 10 Myr than the present age estimates based on CMDs.

(iii) Assuming an LMC distance modulus of 18.5 mag, the derived reddening for the clusters in our sample is consistent with that derived from H I emission and 100-μm all-sky dust maps.

(iv) In the mass range of 2–12 $M_\odot$, the MF slopes for eight out of nine sample clusters were found to be similar, with values of γ ranging from -1.90 ± 0.16 to -2.28 ± 0.21. For NGC 1767 the slope was found to be significantly shallower, with $\gamma = -1.23 \pm 0.25$. The present MF values are consistent with those derived by Dieball & Grebel (1998) for NGC 2006 and SL 538. Selman & Melnick (2005) studied the star formation history and IMF of the field population of the 30 Doradus super association and found that it has a Salpeter slope in the mass range of 7 to 40 $M_\odot$.

(v) the MF slopes of the inner and outer cluster regions indicate the presence of mass segregation in NGC 2002, 2006, 2136

Table 7. Luminosity functions for the sample LMC star clusters. The columns denote: (1) *V* magnitude of the bin centre – 0.5 mag is taken as the bin width; (2) mass of the bin centre as read from the best-fitting isochrones in $M_{\odot}$; (3)–(10) completeness factor (CF) and number of stars (NS) in the bin for the 'Ring 1', 'Ring 2' and 'Total' cluster regions as well as the corresponding field region; (11)–(13) the derived cluster luminosity function for the above three regions of the cluster after correcting for data incompleteness and field-star contamination. For NGC 2098, the luminosity function could not be derived for the outer region because of poor statistics.

Bin	Bin	Ring 1		Ring 2		Total		Field region		Ring 1	Ring 2	Total
(*V* mag)	($M_{\odot}$)	CF	NS	CF	NS	CF	NS	CF	NS	LF	LF	LF
(1)	(2)	(3)	(4)	(5)	(6)	(7)	(8)	(9)	(10)	(11)	(12)	(13)
NGC 1767												
15.25	10.83	1.00	2	1.00	1	1.00	3	1.00	0	2.00	1.00	3.00
15.75	10.19	1.00	5	1.00	2	1.00	7	1.00	1	4.80	1.42	6.22
16.25	9.45	1.00	4	1.00	2	1.00	6	1.00	2	3.60	0.84	4.44
16.75	8.56	1.00	10	1.00	5	1.00	15	1.00	1	9.80	4.42	14.22
17.25	7.57	1.00	9	1.00	3	1.00	12	1.00	3	8.40	1.26	9.66
17.75	6.52	1.00	9	1.00	6	1.00	15	1.00	4	8.21	3.68	11.88
18.25	5.50	0.99	22	1.00	6	0.98	28	1.00	4	21.43	3.68	25.45
18.75	4.56	0.97	16	1.00	13	0.96	29	0.99	20	12.48	1.26	14.46
19.25	3.74	0.94	19	0.99	19	0.94	38	0.97	25	15.10	4.21	20.33
19.75	3.06	0.89	8	0.90	24	0.88	32	0.88	23	–	11.48	15.99
NGC 1994												
15.25	12.09	1.00	2	1.00	2	1.00	4	1.00	0	2.00	2.00	4.00
15.75	11.08	1.00	4	1.00	8	1.00	12	1.00	1	3.79	6.02	9.81
16.25	9.90	1.00	2	1.00	12	1.00	14	1.00	1	1.79	10.02	11.81
16.75	8.64	1.00	2	1.00	12	1.00	14	1.00	3	1.36	6.06	7.42
17.25	7.40	1.00	7	1.00	17	1.00	24	1.00	8	5.30	1.15	6.45
17.75	6.22	1.00	9	1.00	12	1.00	21	1.00	2	8.57	8.04	16.61
18.25	5.15	1.00	14	1.00	38	1.00	52	1.00	11	11.66	16.21	27.87
18.75	4.21	0.99	25	0.99	42	0.98	67	0.99	14	22.24	14.41	37.34
19.25	3.42	0.96	35	0.97	67	0.96	102	0.96	18	32.47	31.92	65.11
19.75	2.79	0.82	29	0.90	91	0.86	120	0.92	34	27.50	27.89	58.45
NGC 2002												
15.25	11.99	1.00	4	1.00	6	1.00	10	1.00	5	3.67	2.88	6.55
15.75	11.24	1.00	8	0.96	6	1.00	14	1.00	3	7.80	4.38	11.93
16.25	10.29	1.00	4	1.00	13	1.00	17	1.00	7	3.53	8.64	12.17
16.75	9.19	0.99	3	1.00	16	0.99	19	1.00	15	2.03	6.65	8.84
17.25	8.02	0.96	14	0.98	15	0.98	29	0.96	13	13.68	6.87	20.24
17.75	6.85	0.90	11	0.88	23	0.88	34	0.94	11	11.44	18.84	30.56
18.25	5.75	0.80	16	0.82	31	0.80	47	0.88	19	18.55	24.35	43.85
18.75	4.74	0.58	17	0.62	40	0.62	57	0.82	36	26.37	37.15	61.63
19.25	3.87	0.45	11	0.56	65	0.54	76	0.76	67	18.54	61.12	79.89
19.75	3.16	0.40	13	0.46	63	0.45	76	0.62	64	25.59	72.62	97.64
NGC 2003												
15.25	10.06	1.00	2	1.00	3	1.00	5	1.00	0	2.00	3.00	5.00
15.75	9.43	1.00	3	1.00	4	1.00	7	1.00	0	3.00	4.00	7.00
16.25	8.73	1.00	2	1.00	5	1.00	7	1.00	2	1.76	2.38	4.14
16.75	7.88	1.00	6	1.00	9	1.00	15	1.00	1	5.88	7.69	13.57
17.25	6.93	1.00	12	1.00	14	1.00	26	1.00	1	11.88	12.69	24.57
17.75	5.94	1.00	14	1.00	9	1.00	23	1.00	1	13.88	7.69	21.57
18.25	4.99	1.00	20	1.00	28	1.00	48	1.00	1	19.88	26.69	46.57
18.75	4.12	0.99	28	1.00	34	1.00	62	1.00	8	27.33	23.53	50.58
19.25	3.37	0.96	26	1.00	43	0.99	69	0.99	11	25.77	28.45	53.83
19.75	2.76	0.86	30	0.98	68	0.96	98	0.98	19	32.59	44.01	74.40
20.25	2.27	0.78	20	0.90	91	0.86	111	0.96	30	–	60.20	84.46
NGC 2006												
15.25	9.88	0.99	3	0.99	3	0.99	6	1.00	2	2.91	2.66	5.57
15.75	9.27	0.94	5	0.96	1	0.95	6	1.00	3	5.14	0.48	5.58
16.25	8.52	0.91	7	0.92	2	0.92	9	1.00	6	7.33	1.06	8.30
16.75	7.65	0.88	8	0.91	5	0.90	13	0.99	4	8.85	4.74	13.45
17.25	6.68	0.85	13	0.88	4	0.84	17	0.99	14	14.44	1.91	16.75
17.75	5.70	0.80	8	0.83	8	0.82	16	0.98	7	9.57	8.31	17.75
18.25	4.76	0.73	16	0.80	17	0.76	33	0.96	26	20.28	16.20	36.74
18.75	3.92	0.68	10	0.78	11	0.73	21	0.92	26	13.00	8.84	21.79
19.25	3.21	0.61	12	0.70	23	0.66	35	0.88	39	17.00	24.60	42.09
19.75	2.64	0.45	10	0.64	20	0.54	30	0.82	44	18.98	21.25	42.31

Table 8 – *continued*

Bin (V mag) (1)	Bin ($M_\odot$) (2)	Ring 1 CF (3)	NS (4)	Ring 2 CF (5)	NS (6)	Total CF (7)	NS (8)	Field Region CF (9)	NS (10)	Ring 1 LF (11)	Ring 2 LF (12)	Total LF (13)
SL 538												
15.25	10.86	1.00	1	1.00	2	1.00	3	1.00	2	0.89	1.71	2.61
15.75	10.06	0.99	1	1.00	4	1.00	5	1.00	3	0.85	3.57	4.41
16.25	9.08	0.98	2	0.99	2	1.00	4	1.00	6	1.72	1.16	2.82
16.75	8.01	0.97	6	0.98	10	0.99	16	0.99	4	5.97	9.62	15.36
17.25	6.90	0.96	5	0.96	3	0.95	8	0.99	14	4.44	1.10	5.63
17.75	5.83	0.94	9	0.94	10	0.94	19	0.98	7	9.19	9.61	18.80
18.25	4.84	0.91	8	0.90	12	0.90	20	0.96	26	7.33	9.45	16.87
18.75	3.96	0.88	10	0.86	11	0.87	21	0.92	26	9.84	8.74	18.56
19.25	3.23	0.82	12	0.78	16	0.74	28	0.88	39	12.24	14.15	29.09
NGC 2011												
15.75	10.16	1.00	5	1.00	9	1.00	14	1.00	2	4.72	–	11.18
16.25	9.20	1.00	5	1.00	5	1.00	10	1.00	2	4.72	–	7.18
16.75	8.14	1.00	3	1.00	5	1.00	8	1.00	4	2.44	–	2.37
17.25	7.04	0.99	6	1.00	10	1.00	16	1.00	5	5.36	3.66	8.96
17.75	5.96	0.98	2	1.00	12	1.00	14	1.00	4	1.48	6.93	8.37
18.25	4.95	0.96	10	0.99	20	0.99	30	1.00	6	9.58	12.60	21.86
18.75	4.06	0.95	10	0.98	30	0.98	40	0.99	9	9.25	19.09	28.02
19.25	3.31	0.90	19	0.95	39	0.95	58	0.98	14	19.11	22.94	40.94
19.75	2.71	0.87	18	0.91	54	0.93	72	0.96	33	15.88	15.77	29.03
NGC 2098												
15.75	8.56	1.00	6	1.00	1	1.00	7	1.00	7	5.29	–	3.91
16.25	8.03	1.00	5	1.00	2	1.00	7	1.00	8	4.18	–	3.47
16.75	7.35	1.00	7	1.00	6	1.00	13	1.00	16	5.37	–	5.93
17.25	6.53	1.00	10	1.00	5	1.00	15	1.00	18	8.16	–	7.05
17.75	5.65	1.00	14	1.00	10	1.00	24	1.00	30	10.94	–	10.75
18.25	4.78	0.99	24	0.99	8	0.99	32	1.00	36	20.57	–	16.42
18.75	3.96	0.98	21	0.98	10	0.98	31	1.00	35	17.85	–	16.17
19.25	3.26	0.96	28	0.97	23	0.97	51	1.00	54	23.65	–	28.73
19.75	2.68	0.83	26	0.94	28	0.93	54	0.99	59	25.24	–	31.74
20.25	2.21	0.74	22	0.88	43	0.88	65	0.96	66	22.71	–	43.50
NGC 2136												
16.75	5.29	1.00	12	1.00	4	1.00	16	1.00	0	12.00	4.00	16.00
17.25	5.02	1.00	14	1.00	18	1.00	32	1.00	3	13.75	16.19	29.94
17.75	4.65	1.00	33	1.00	20	1.00	53	1.00	3	32.75	18.19	50.94
18.25	4.19	0.99	49	1.00	41	1.00	90	1.00	2	49.33	39.79	88.63
18.75	3.65	0.96	65	0.99	55	0.98	120	1.00	6	67.21	51.94	118.33
19.25	3.12	0.94	70	0.97	74	0.97	144	0.98	8	73.78	71.37	142.85
19.75	2.63	0.86	59	0.96	111	0.94	170	0.97	21	66.79	102.58	165.99

and 2098. For NGC 2098, Kontizas et al. (1998) derive the dynamical relaxation time, T_e, to be between 640 and 1050 Myr. This may indicate that the value of T_e for LMC star clusters could be few hundred million years. The ages of LMC star clusters under study are therefore significantly smaller than their dynamical relaxation time. Consequently, observed mass segregation in these clusters is probably primordial in nature. A compilation of both ground- and space-based observations of extremely young galactic and MC star clusters (cf. Hunter et al. 1995; Sagar et al. 1988; Hillenbrand & Hartmann 1998; Chen et al. 2007, and references therein) indicates the presence of mass segregation in most of them, although to varying degrees. All these indicate that for most young star clusters located in different galaxies mass segregation effects are observed and are probably the imprint of star formation processes.

(vi) A mean MF slope of $\gamma = -2.22 \pm 0.16$ derived for a sample of 25 young (<100 Myr) stellar systems in the LMC provides support for the universality of the IMF in the intermediate-mass range $\sim$2–10 $M_\odot$. An IMF study of the 30 Doradus star-forming region of the LMC by Selman & Melnick (2005) supports this conclusion.

ACKNOWLEDGMENTS

The authors are grateful to the anonymous referee for constructive comments. Useful discussions with Drs K.S. de Boer, P. Kroupa and T. Richtler are gratefully acknowledged. We thank Dr Vijay Mohan for help in data reduction. One of us (RS) would like to thank the Alexander von Humboldt Foundation, Bonn for providing financial support for him to work at the Sterwarte/Argelander Institute of Astronomy in Bonn. BK acknowledges support from the Chilean Centre for Astrophysics FONDAP No. 15010003. This work is based on observations collected at the European Southern Observatory, Chile.

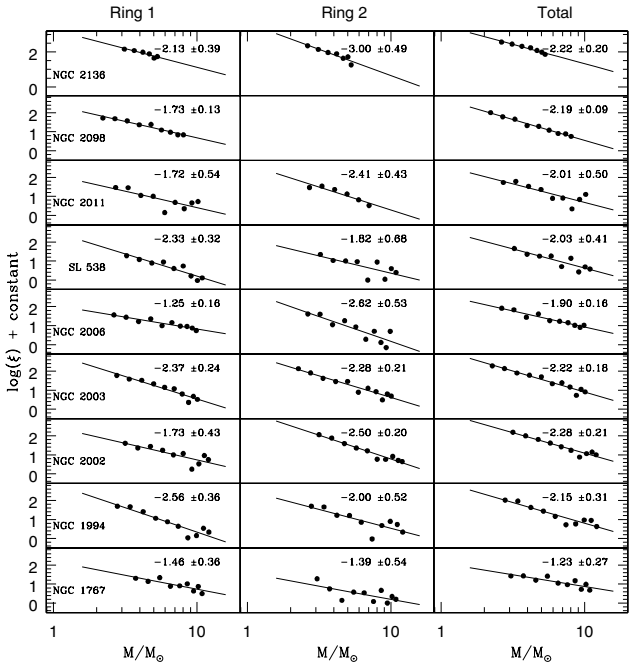

Figure 14. MFs derived using Girardi et al. (2002) isochrones for 'Ring 1', 'Ring 2' and 'Total' cluster region are shown with solid circles. Solid lines denote the best-fitting straight lines, with the values of slopes displayed in the respective panels. As a result of poor statistics, the MF could not be derived for the outer region of NGC 2098.

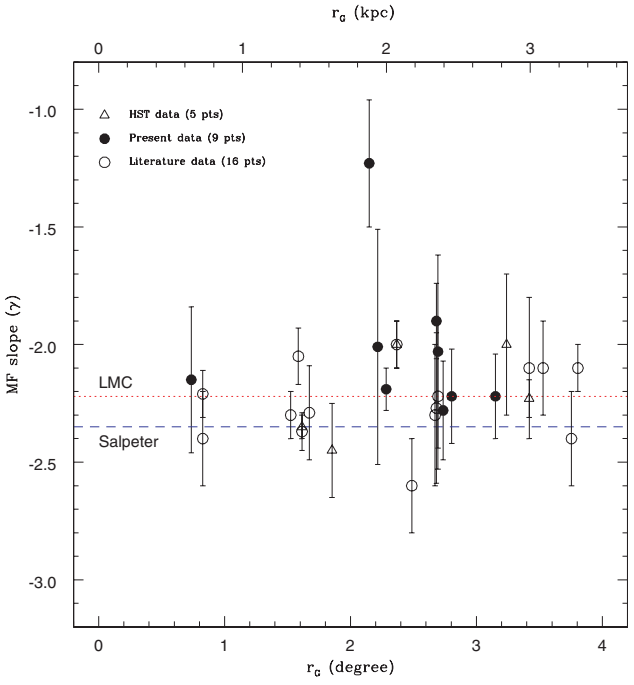

Figure 15. Plot of MF slopes against the galactocentric distance (r_G) in the LMC. Including estimates from the literature (see text), the MF slopes for 26 young (<100 Myr) star clusters and associations are shown. The horizontal dashed line represents the Salpeter (1955) value of the IMF slope for the field stars in the solar neighbourhood, and the dotted line indicates the mean slope for a sample of 25 (excluding one outlier) LMC star clusters and associations.

REFERENCES

Alves D. R., 2004, Nat, 48, 659
Burstein D., Heiles C., 1982, AJ, 87, 1165
Bessell M. S., 1991, A&A, 242, L17
Bhatia R. K., 1992, Mem. Soc. Astron. Ital., 63, 141
Bica E., Schmitt H. R., 1995, ApJS, 101, 41
Bica E., Claria J. J., Dottori H., Santos J. F. C., Jr., Piatti A. E., 1996, ApJS, 102, 57
Bica E. L. D., Schmitt H. R., Dutra C. M., Oliveira H. L., 1999, ApJ, 117, 238
Böhm-Vitense E., Canterna R., 1974, ApJ, 194, 629
Brocato E., Di Carlo E., Menna G., 2001, A&A, 374, 523
Chen L., De Grijs R., Zhao J. L., 2007, AJ, 134, 1368
Dieball A., Grebel E. K., 1998, A&A, 339, 773
Dieball A., Mueller H., Grebel E. K., 2002, A&A, 391, 547
Dirsch B., Richtler T., Gieren W. P., Hilker M., 2000, A&A, 360, 133
Elmegreen B. G., 2000, ApJ, 539, 342
Elson R. A. W., Fall S. M., 1985, ApJ, 299, 211
Girardi L., Bertelli G., Bressan A., Chiosi C., Groenewegen M. A. T., Marigo P., Salasnich B., Weiss A., 2002, A&A, 391, 195
Gouliermis D. A., Lianou S., Kontizas M., Kontizas E., Dapergolas A., 2006, ApJ, 652, L93
Hilker M., Richtler T., Stein D., 1995, A&A, 299, L37
Hillenbrand L. A., Hartmann L. E., 1998, ApJ, 492, 540
Hunter D. A., Shaya E. J., Holtzman J. A., Light R. M., O'Neil E. J., Jr., Lynds R., 1995, ApJ, 448, 179
Kerber L. O., Santiago B. X., Brocato E., 2007, A&A, 462, 139
Kjeldsen K., Frandsen S., 1991, A&AS, 87, 119
Kontizas M., Hatzidimitriou D., Bellas-Velidis I., Gouliermis D., Kontizas E., Cannon R. D., 1998, A&A, 336, 503
Kroupa P., 2001, MNRAS, 322, 221
Kumar B., Sagar R., Sanwal B. B., Bessell M., 2004, MNRAS, 353, 991
Landolt A. U., 1992, AJ, 104, 340.
Larson R. B., 1998, MNRAS, 301, 569
Mackey A. D., Gilmore G. F., 2003, MNRAS, 338, 85
Matteucci A., Ripepi V., Brocato E., Castellani V., 2002, A&A, 387, 861
Rolleston W. R. J., Trundle C., Dufton P. L., 2002, A&A, 396, 53
Sagar R., 1987, MNRAS, 228, 483
Sagar R., 1993, Current Science, 64, 293
Sagar R., 1995, Bull. Astron. Soc. India, 23, 433
Sagar R., 2000, Bull. Astron. Soc. India, 28, 55
Sagar R., 2002, in Geisler D., Grebel E. K., Minniti D., eds, Proc. IAU Symp. 207, Extragalactic Star Clusters. Kluwer, Dordrecht, p. 515
Sagar R., Joshi U. C., 1978, Bull. Astron. Soc. India, 6, 37
Sagar R., Richtler T., 1991, A&A, 250, 324
Sagar R., Myakutin V. I., Piskunov A. E., Dluzhnevskaya O. B., 1988, MNRAS, 234, 831
Sagar R., Richtler T., de Boer K. S., 1991, A&AS, 90, 387
Salpeter E. E., 1955, ApJ, 121, 161
Schaefer B. E., 2008, AJ, 135, 112
Schlegel D. J., Finkbeiner D. P., Davis M., 1998, ApJ, 500, 525
Searle L., Wilkinson A., Bagnuolo W. G., 1980, ApJ, 239, 803
Selman F. J., Melnick J., 2005, A&A, 443, 851
Shapley H., Lindsay E. M., 1963, Ir. Astron. J., 6, 74
Stetson B., 1987, PASP, 99, 191
Stetson P. B., 1992, JRASC, 86, 71
Subramaniam A., Sagar R., 1999, AJ, 117, 937
Sulentic J. W., Tifft W. G., 1973, Revised New General Catalogue of Nonstellar Astronomical Objects. Univ. Arizona Press, Tucson
Wolf M. J., Drory N., Gebhardt K., Hill G. J., 2007, ApJ, 655, 179
Yadav R. K. S., Sagar R., 2001, MNRAS, 328, 370

SUPPLEMENTARY MATERIAL

The following supplementary material is available for this article:

Table 4. The relative positions (X, Y), CCD magnitude (V) and colours ($B - V, V - R$ and $V - I$) of all the stars measured in cluster and nearby field regions are presented sequentially for the clusters NGC 1767, 1994, 2002, 2002F, 2003, 2006 (including SL 538), 2011, 2098, 2136 and 2136F. Along with the star identification (ID), the cluster or field region identification is also provided in the first column.

This material is available as part of the online article from: http://www.blackwell-synergy.com/doi/abs/10.1111/j.1365-2966.2008.12926.x (This link will take you to the article abstract.)

Please note: Blackwell Publishing is not responsible for the content or functionality of any supplementary materials supplied by the authors. Any queries (other than missing material) should be directed to the corresponding author for the article.

This paper has been typeset from a TEX/LATEX file prepared by the author.